Ligand Rearrangement Reactions of $Cr(CO)_6$ in Alcohol Solutions: Experiment and Theory

Jennifer E. Shanoski, Elizabeth A. Glascoe, and Charles B. Harris*

Department of Chemistry, University of California, Berkeley, California 94720, and Chemical Sciences Division, E. O. Lawrence Berkeley National Laboratory, Berkeley, California 94720

Received: October 3, 2005; In Final Form: November 10, 2005

The ligand rearrangement reaction of $Cr(CO)_6$ is studied in a series of alcohol solutions using ultrafast infrared spectroscopy and Brownian dynamics simulations. Excitation with 266 nm light gives $Cr(CO)_5$ which is quickly solvated by a ligand from the bath. In alcohol solutions, solvation by an alkyl or hydroxyl site can occur; all alkyl bound complexes eventually rearrange to hydroxyl bound complexes. This rearrangement has been described using both an intermolecular (stochastic) and intramolecular (chainwalk) mechanism. Experiments alone do not allow for characterization of the mechanism, and therefore, theoretical calculations were carried out for the first time by modeling the ligand rearrangement as a diffusive walk along a potential defined by the different interaction possibilities. Experiments and simulations were carried out for $Cr(CO)_6$ in 1-propanol, 2-propanol, 1-butanol, 2-butanol, isobutanol, 1-pentanol, 2-pentanol, 2-methylbutanol, and 3-methylbutanol. The trends in the theoretical and experimental rearrangement times are similar for all simulations carried out indicating that the two mechanisms have very similar ensemble behavior when bath effects are taken into account. The nature of the mechanism responsible for motion along the alcohol chain is not of primary importance in isolating the kinetic behavior because of the highly diffusive nature of the reaction. Future experimental and theoretical work will be directed at identifying a definitive assignment of the reaction mechanism.

1. Introduction

Ligand exchange reactions involve both the fundamental solvation of photochemically prepared transient species and the rearrangement of such species to synthetically important products. In general terms, ligand exchange describes any reaction in which a bound ligand is exchanged for another ligand molecule of the same or of different chemical composition. Traditionally, such reactions are given mechanistic descriptions of dissociative, associative, and dissociative interchange.[1] In a dissociative mechanism, the first step in ligand exchange is the dissociation of a bound ligand from the metal center followed by association of an incoming ligand from the surrounding solvent shell. In an associative mechanism these steps are reversed; a solvent molecule partially associates with the metal center causing the bound ligand to dissociate. A dissociative interchange mechanism is a hybrid of the other two; the association of a solvent molecule is concomitant with the dissociation of the initially bound ligand. Many researchers have focused their attention on determining the most appropriate label for a specific reaction sequence using kinetic data, but such a determination can be difficult due to the similarity in the kinetic behavior observed for these processes. In fact, it is questionable whether such a distinction is possible with ensemble measurements.[2]

A similar focus has been directed toward linkage isomerization reactions where the solvent molecule offers more than one bonding site to the unsaturated metal.[3−5] The steps involved in this type of ligand exchange reaction are not well defined in the context of traditional ligand exchange mechanistic descriptions. In the current work, we examine the dynamics of linkage isomerization reactions of $Cr(CO)_6$ in neat alcohol solutions. Upon photoirradiation, the unsaturated metal center is solvated within 1−2 ps to form a species that is bound either to one of the alkyl groups or to the hydroxyl group. The interaction between the metal center and the alkyl group is weak, and rearrangement from the alkyl bound complex to the hydroxyl bound complex is observed as shown in Figure 1. The alkyl interaction itself is an instructive starting point for understanding the nature of the rearrangement.

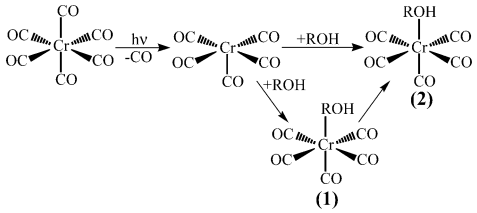

Figure 1. Photochemical reaction of chromium hexacarbonyl in a neat alcohol solution after photoexcitation. The first solvated species can be either alkyl (1) or hydroxyl (2) solvated. Eventually, all alkyl solvated complexes will become hydroxyl solvated species.

When a group 6 metal pentacarbonyl is prepared in a neat alkane solution, the alkyl group serves as a "token" ligand in which the interaction between the metal center and the alkyl solvent is very weak.[6] These complexes have been observed in ambient solutions using a variety of techniques including infrared spectroscopy and nuclear magnetic resonance (NMR). NMR studies have indicated that the site of binding to the metal center changes with time and that the interaction is not static.[7] In a neat alkane solvent, this weakly solvated complex continues to exist in solution until a carbonyl group diffuses into the first solvation shell. The more strongly binding carbonyl group will replace the weakly bound alkyl solvent resulting in regeneration of the parent species.

In an alcohol solvent, however, the hydroxyl group serves as a stronger binding site and will always be in close proximity to the metal center. Consequently, the weakly solvated alkyl-metal complexes will eventually turn over into the thermody-

10.1021/jp055636x CCC: $33.50
Published on Web 12/21/2005

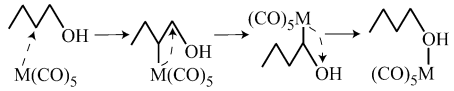

Figure 2. Schematic representation of the intramolecular rearrangement or chainwalk mechanism.

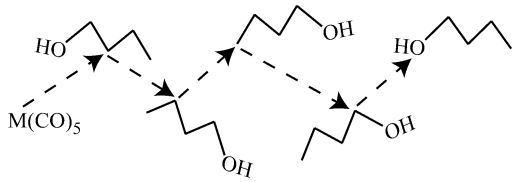

Figure 3. Schematic representation of the intermolecular rearrangement or stochastic mechanism.

namically more stable hydroxyl solvated complexes before diffusive motion brings a carbonyl group in close contact to the metal center. At times after the initial solvation, but before the final product formation, the various alkyl sites of the solvent can be sampled by the metal center. As a result, reactions of this type will have dynamics that reflect this exchange: longer chain alcohols will have final product formation time constants that are much longer than short chain alcohols. For example, $Cr(CO)_6$ in neat ethanol forms the hydroxyl solvated complex within 25 ps while $Cr(CO)_6$ in neat hexanol forms the similar complex in approximately 1.8 ns.[8] The sampling of alkyl sites is a central aspect of the microscopic nature of these reactions.

Instead of simply characterizing the mechanism as dissociative, associative, or dissociative interchange, it has been suggested that such a reaction should be considered in terms of intermolecular versus intramolecular rearrangement. Two general mechanisms have been presented in the literature to explain the mechanism of this rearrangement process. The intramolecular chainwalk mechanism, depicted in Figure 2, is one common description of this reaction.[5,9] The initial binding of a solvent molecule in the first 1−2 ps after photolysis is expected to be random as described above. If this initial solvation is to an alkyl site, the molecule will rearrange by walking along the alkyl backbone until it reaches the hydroxyl site at which point rearrangement ceases. Alternatively, an intermolecular mechanistic description, depicted in Figure 3 has been suggested where the initially solvated metal complex rearranges through complexation with a new solvent molecule.[4,10,11] This process can occur via an associative, dissociative, or interchange mechanism. The newly bound complex, however, will be bound to a new solvent molecule in some new random orientation or position along the alcohol chain. This can be considered a stochastic process since the sampling of solvent sites is expected to be random in contrast to the more systematic chainwalk mechanism. The stochastic rearrangement ends when a hydroxyl site is eventually found as in the chainwalk description.

To gain a more definitive understanding of the particular form of the rearrangement mechanism, it is necessary to determine whether the two standard descriptions are actually distinguishable. Toward this end, we have undertaken a comprehensive study of this reaction using experiments and numerical simulations. The numerical simulations of the dynamics for both the stochastic and chainwalk mechanisms are based on the Langevin equation. Such simulations have been utilized for a variety of chemical processes that range from simple isomerization reactions[12] to protein folding dynamics.[13] The underlying physical picture for these simulations is that the solvent can provide energy to or take energy from the chemical system; this transfer of energy can result in a chemical change. The fluctuating force is related to the friction coefficient which is characterized by the solvent viscosity. The bulk viscosity is derived from the microscopic fluctuations of particle velocity. These simulations therefore utilize a bulk property to characterize the microscopic details of a chemical reaction.

The current work uses these techniques to model complex organometallic rearrangement dynamics for the first time and compares the results to ultrafast, ultraviolet pump, infrared probe experimental data. These simulations are, to our knowledge, the first aimed at elucidating the nature of this ubiquitous rearrangement process. We demonstrate that these two models are nearly indistinguishable due to the broad distribution of initial sites and the highly diffusive nature of the reaction which results in a large sampling of sites for both mechanistic descriptions.

2. Methods

The experimental apparatus utilized in these experiments has been described in detail elsewhere.[14] Briefly, the output of a commercial, regeneratively amplified, Ti:sapphire oscillator (SpectraPhysics) is split into two beam lines. The first is tripled to obtain a 266 nm pump beam. The second is sent into a home-built optical parametric amplifier to generate tunable infrared (3.0−6.0 μm) probe pulses. The infrared probe pulse is split into signal and reference beams in order to account for shot-to-shot noise of the laser system. The signal beam is directed into a sample cell at a well-defined time after the pump pulse has arrived at the sample. The time delay between the pump and probe pulses is controlled by a translational stage (Klinger) positioned in the pump beam line. The signal and reference lines are then dispersed in a spectrograph and sent to a 32×2 element array detector. The data are then collected and analyzed via computer-controlled data acquisition. The sample is flowed through the cell in order to ensure that fresh sample is photolyzed with each laser shot. The cell is moved perpendicular to the beam incident angle to avoid burning effects which can mask or enhance absorptions from photoproducts. This experimental apparatus provides a spectral resolution of 4 cm^{-1} and a temporal resolution of 150 fs. Absorption changes as small as 50 μOD can be observed with 1.0 s of signal collection time.

All spectroscopic grade solvents and $Cr(CO)_6$ were purchased from Sigma-Aldrich and used without further purification. Experimental samples were prepared by dissolving $Cr(CO)_6$ in the appropriate solvent to obtain a concentration of 10−15 mM; solutions were filtered before use to remove any undissolved metal.

Both alkyl and hydroxyl solvated species are observed in the experimental data. It is therefore possible to consider the spectra in long chain alcohols as the sum of contributions from the two different solvated metal species. Raw spectra from $Cr(CO)_6$ in pentane and $Cr(CO)_6$ in methanol were used in the determination of time constants for $Cr(CO)_6$ in each alcohol. The spectra of $Cr(CO)_6$ in pentane and $Cr(CO)_6$ in methanol at a given time were each multiplied by a constant value and added together according to the following expression

$$\nu(\tau_i)_{\mathrm{ROH}} = A^*\nu(\tau_i)_{\mathrm{methanol}} + B^*\nu(\tau_i)_{\mathrm{pentane}} \qquad (1)$$

where $\nu(\tau_i)$ is the spectrum of the alcohol or pentane at time τ_i and A and B are adjustable parameters. An example of a fit for 1-butanol using this method is shown in Figure 4. Methanol was used to fit the hydroxyl peak because spectra of $Cr(CO)_6$ in methanol only show a hydroxyl solvated complex at all delay times after photoexcitation; no rearrangement is observed. Values of A and B were determined using a chi-squared fitting routine to fit the spectrum of the alcohol of interest with the sum of the spectra of methanol and pentane at the same time

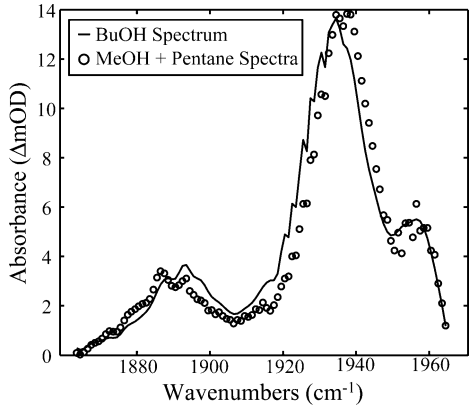

Figure 4. Spectrum of $Cr(CO)_5$ in 1-butanol 700 ps after photoexcitation (solid lines) overlayed with the sum of spectra from $Cr(CO)_5$ in methanol and pentane (open circles). The fitting routine adjusts for intensity but does not incorporate shifts in the absorption frequency. Differences in the absorption frequency of 5 cm^{-1} are encountered due to solvent differences.

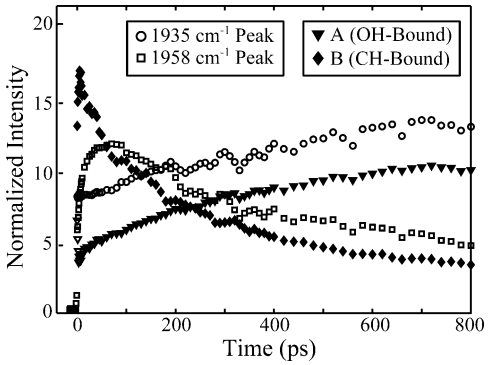

Figure 5. Comparison of kinetic traces resulting from eq 1 (solid diamonds and triangles) and raw data (open circles and squares) for 1-butanol. The exponential rise (hydroxyl solvated species) and decay (alkyl solvated species) are well reproduced. The early time vibrational relaxation is minimized by utilizing eq 1, and the rearrangement dynamics are isolated.

slice. This was repeated for all of the experimental time slices. This method allowed for the minimization of vibrational relaxation and overlap effects which served to mask the absorptions. The values of the constants were plotted against the time at which the spectra were taken and fit using either a single or double exponential function to measure the rise of the absorption due to hydroxyl solvation and the decay of the absorption due to alkyl solvation. The kinetic data obtained in this fashion were compared with raw experimental traces and were found to agree well numerically, but with decreased scatter as expected. A comparison of the raw kinetic data to the kinetic data from fitting is shown in Figure 5. All kinetic data given for long chain alcohols are the result of this fitting routine. All other data, including spectra, are raw data. Errors in the exponential fits to the data are 95% confidence intervals.

For the computational work, simulations based on the Langevin equation (more detail in section 3 below) require well depths for the different alkyl and hydroxyl binding sites. To that end, metal−ligand binding energies were calculated with density functional theory (DFT) using the Gaussian03 suite.[15] Becke's three-parameter exchange correlation energy[16] combined with the Lee−Yang−Par correlation functional,[17] B3LYP,[18] was used in all calculations. The basis set used for the main group elements consisted of the 6-311G** basis functions,[19,20] and the LANL2DZ core potential[21] was used for all of the central transition metals. Frequency calculations were carried out in order to ensure that optimized geometries corresponded

TABLE 1: Table of Metal−Ligand Binding Energies Calculated Using Density Functional Theory[a]

	binding energy (kcal/mol)					
alcohol	M−OH	M−C_α	M−C_β	M−$C\gamma$	M−C_δ	M−C_ϵ
1-propanol	16.53	5.62	5.22	3.71		
2-propanol	15.69	5.47	4.26	4.26		
1-butanol	16.40	5.43	5.07	3.27	3.67	
2-butanol	15.50	5.47	4.87	3.84		
			3.14			
isobutanol	16.21	5.22	5.43	3.54		
1-pentanol	16.42	5.47	5.14	2.90	3.37	3.89
2-pentanol	16.51	5.51	4.66	2.84	3.96	
			3.19			
2-methylbutanol	16.65	5.55	4.88	3.58	4.04	
				4.11		
3-methylbutanol	16.61	5.84	5.64	4.10	3.96	

[a] Labels for the various alkyl sites on the alkyl chain represent the distance from the hydroxyl site. Entries with multiple binding energies are found for asymmetric branched alcohols.

to minima on the potential energy surface. Each of the solvated species were analyzed for signature infrared absorptions and energies. The geometries of the individual fragments, ligand, and metal pentacarbonyl center, were optimized, and single point energy calculations were carried out. The bond energies reported here are the result of subtracting the single point energy values of both fragments from the energy of the complex. This method takes zero point energy into account but does not maintain a consistent basis set throughout the calculations. Thus, reported bond energies are not to be viewed as accurate but do provide an estimate of the actual values.

The Langevin simulation results were analyzed in sets of 500 trajectories each. Each set was binned according to the amount of time required for each particle to become trapped in the hydroxyl well. The number of hydroxyl-solvated products was plotted against time, and the data were fit using a single exponential function. This was done independently for 10 trajectory sets (5000 trajectories total). The reported errors in simulation time constants are derived from the standard deviation of those fit constants over the 10 sets.

3. Model Details

Condensed phase reaction dynamics have many unique properties derived from their environment. One such property, energy exchange through collisions, is exploited in the simulations carried out in the current investigation. Here a solvated metal center can become unsaturated if the metal−ligand binding energy is weak enough to be perturbed by collisions from the bath. The binding energy of heptane to $Cr(CO)_5$ has been experimentally measured by Burkey and co-workers using photoacoustic calorimetry to be 9.8 ± 2.2 kcal/mol.[22] Thus, the rearrangement from a weakly bound alkyl complex to a strongly bound hydroxyl complex is considered in the context of energy exchange with the bath.

We model the system of intermolecular exchange using diffusive motion over a barrier. The barrier is defined according to the binding energy of the specific carbon or hydroxyl group that the metal can coordinate to; this value is calculated using DFT as explained in the Experimental Section. For calculation simplicity, we construct a one-dimensional (1-D) potential using a cosine function (from 0 to π). The well depth is adjusted so that it has a maximum value of zero and a minimum value that corresponds to the bond energy of the metal fragment with the alcohol site of interest. Table 1 gives the calculated bond energies for all of the solvent systems studied. The width of the potential well is set to be 3.0 Å for each of the sites; this

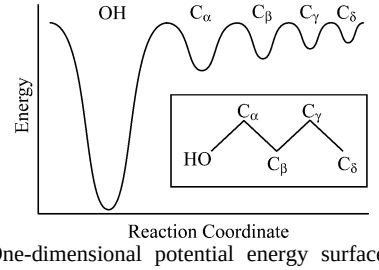

Figure 6. One-dimensional potential energy surface used in the simulation of rearrangement dynamics for $Cr(CO)_6$ in butanol. All other alcohol solutions have the same form of the potential energy surface and vary only in the number and depth of the various wells.

value corresponds to the average distance between binding sites along the alcohol. The 1-D potential surface used for 1-butanol is shown in Figure 6. A more complicated model for the potential of mean force will affect all of the binding sites and will, therefore, change the overall rearrangement time but should not affect the trend when comparing different solvents. Since these simulations are aimed at uncovering the trend in rearrangement times for a number of alcohol solutions, they are not expected to give exact agreement with the experimentally obtained time constants and a more complicated model for the potential energy surface is not needed.

The motion along the potential energy surface is dictated by the Langevin equation

$$m\dot{v}(t) = -\xi m v(t) + R(t) \tag{2}$$

where m is the mass of the metal fragment,[23] ξ is the friction coefficient, $R(t)$ is the fluctuating force, and $v(t)$ is the velocity.[24] The friction coefficient is representative of the frictional force from the solvent acting against the particle motion. The fluctuating force is random and results from collisions between the metal fragment and the solvent; it has zero mean and is uncorrelated to the particle velocity

$$\langle R(t)\rangle = 0 \tag{3a}$$

$$\langle R(t)\, v(0)\rangle = 0 \tag{3b}$$

In the simulations discussed here, the random force will be considered white noise; the process is Markovian.

The friction coefficient is related to the bulk solvent viscosity, η using Stokes' law

$$\xi = \frac{2\pi\eta d}{m} \tag{4}$$

subject to slip boundary conditions, where d is the Brownian particle diameter and m is the Brownian particle mass. Slip conditions have been shown to be more appropriate for the type of calculations carried out here since it is expected that a saturated metal center will not interact strongly with surrounding solvent species.[25−28] Further, we consider a system where the Brownian particle is of similar size to the solvent molecules. Viscosity values at room temperature[29] were used from a standard reference text.[30]

The initial velocity is selected from a thermal distribution, and the initial position is selected randomly. The position, **r**, and velocity, **v**, after one time step are calculated using the velocity-Verlet algorithm[31]

$$\mathbf{r}(t+\delta t) = \mathbf{r}(t) + c_1\mathbf{v}(t)\delta t + c_2\mathbf{a}(t)\delta t^2 + \delta\mathbf{r}^{\mathrm{G}} \tag{5a}$$

$$\mathbf{v}(t+\delta t) = c_0\mathbf{v}(t) + (c_1 - c_2)\mathbf{a}(t)\delta t + c_2\mathbf{a}(t+\delta t)\delta t + \delta\mathbf{v}^{\mathrm{G}} \tag{5b}$$

where c_0, c_1, and c_2 are dependent on the friction coefficient according to

$$c_0 = e^{\xi\delta t} \tag{6a}$$

$$c_1 = (\xi\delta t)^{-1}(1 - c_0) \tag{6b}$$

$$c_2 = (\xi\delta t)^{-1}(1 - c_1) \tag{6c}$$

and $\delta\mathbf{r}^{\mathrm{G}}$ and $\delta\mathbf{v}^{\mathrm{G}}$ are the random components of the position and velocity, respectively, chosen from a Gaussian bivariate distribution. These random terms both have zero mean, but since they derive from the same random process (collisions with the bath), they are correlated.[31] The correlation is defined

$$\langle(\delta\mathbf{r}^{\mathrm{G}}\delta\mathbf{v}^{\mathrm{G}})\rangle = \delta t k_{\mathrm{B}}T(\xi\delta t)^{-1}(1 - e^{-\xi\delta t})^2 \tag{7}$$

The criterion for the use of this simulation type is that the particle must experience many collisions within the time scale of the dynamics. This criterion is met when

$$\xi\delta t \gg 1 \tag{8}$$

Thus, the time step of 0.500 ps is chosen for these simulations. It is large enough to ensure the validity of this inequality and, at the same time, is small enough to ensure adequate sampling of the trajectories.

Three distinct simulation types were carried out for the rearrangement in each of the solvents studied: stochastic, chainwalk, and biased chainwalk. All three simulation types begin with a randomly chosen velocity and position and utilize the above algorithm to move the particle within a given well. The metal center becomes unbound when it moves beyond the position where the potential is defined for a given site in either the positive or negative direction. The simulation ends when a particle becomes trapped in the hydroxyl well; a trapped particle is defined as being 10 $k_{\mathrm{B}}T$ below the barrier top. The difference between the three simulation types is in the choice of a new site after the metal center has become unbound but before it is trapped. In the first simulation type, the stochastic simulation, after the alkyl bound complex is dissociated from the metal center a new site and a new position in the well that defines the site are randomly chosen. In the second simulation choice, the random chainwalk simulation, dissociation of an alkyl bound complex is followed by movement to an adjacent site and the position will be on the edge of the well. If there is more than one adjacent site, the site is chosen randomly from the possibilities. The third simulation type, the biased chainwalk simulation, is the same as the random chainwalk simulation except that the choice between neighboring sites is weighted by the derivative of the potential energy surface so that the site with the strongest binding energy is most likely. The biased chainwalk simulation represents a rearrangement process that is between the two extremes of pure stochastic and pure chainwalk. The biased chainwalk simulation reflects the possibility that dissociation can occur but that the choice of the next site will be influenced by the previous position and the force from the potential.

The chainwalk and biased chainwalk mechanisms as described are not purely associative as suggested by previous studies.[5,9] Our model is dissociative in nature and cannot, therefore, be used to examine a purely associative mechanism. This is not important because the intermediate complexes are the same in both the associative and dissociative mechanisms and the only difference in the mechanistic descriptions will be

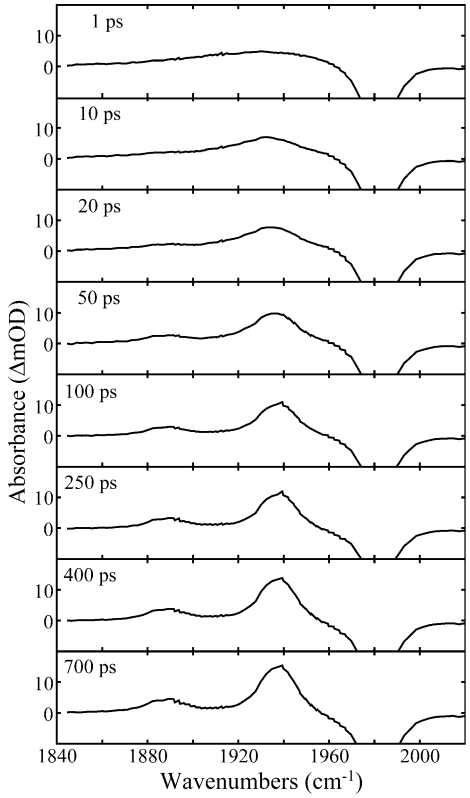

Figure 7. UV-pump, IR-probe spectra of chromium hexacarbonyl in neat methanol at increasing delay times after photoexcitation.

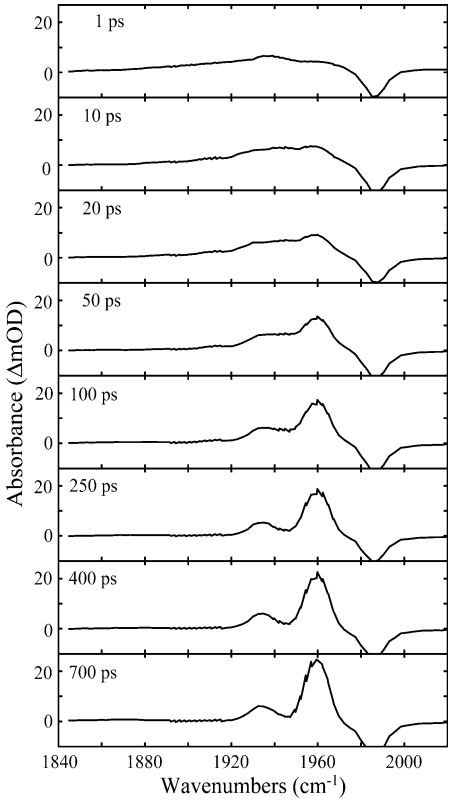

Figure 8. UV-pump, IR-probe spectra of chromium hexacarbonyl in neat pentane at increasing delay times after photoexcitation. The apparent increase in the bleach at long delay times is an experimental artifact.

the transition state of the complex as it moves from one site to another. In our simulations, the transition state will characterize the barrier heights on the potential energy surface and will alter all of the barriers in a similar fashion. Further, all alcohol solvents will have a similar change in the barrier height. Since we are concerned with the trends between the different models as they relate to the experimental data, this limitation in our model is not expected to have a significant contribution.[32]

4. Results

Upon irradiation with 266 nm light, a single carbonyl group dissociates from the parent hexacarbonyl complex within 100 fs.[33] The unsaturated metal center is solvated by a ligand from the bath in 1−2 ps resulting in an 18-electron complex with varying degrees of stability.[34] UV-pump, IR-probe spectra are shown in Figures 7 and 8 for chromium hexacarbonyl in methanol and pentane, respectively, at varying delay times after photoexcitation. Negative absorptions in the figures indicate the depletion of parent molecules and positive absorptions indicate the presence of transient or product species.

In neat methanol, irradiation of $Cr(CO)_6$ results in the behavior shown in Figure 7. Three features are visible in the difference spectra: the parent bleach centered around 1980 cm^{-1}, and two absorptions from the $Cr(CO)_6$−MeOH species at 1887 and 1939 cm^{-1} corresponding to the A_1 and E bands of the hydroxyl solvated complex, respectively. No peaks are observed for the solvation of the metal center with the alkyl portion of the methanol molecule. The absorptions from the hydroxyl solvated species grow in with a time constant of 37.5 ± 5.1 ps, which is consistent with previously reported values of the vibrational relaxation time of the solvated pentacarbonyl complex in methanol.[8]

In neat pentane, Figure 8, only alkyl groups are available to solvate the unsaturated metal center. Again, three distinct features are visible in the difference spectra for $Cr(CO)_6$ in pentane: the parent bleach centered at 1985 cm^{-1} and two absorptions from the $Cr(CO)_5$−pentane species at 1932 and 1960 cm^{-1}, corresponding to the A_1 and E bands of the complex, respectively.[35] These absorptions are shifted from the values associated with $Cr(CO)_5$(MeOH) reflecting the increased electron-donating ability of the hydroxyl group to the metal center. This absorption grows in with a time constant of 43.5 ± 5.5 ps, which is again consistent with previously reported values of the vibrational relaxation time of the solvated pentacarbonyl complex in pentane.[34]

The experiments in neat methanol and pentane exhibit little dynamical behavior: after excitation with 266 nm light, a carbonyl ligand is dissociated, followed by solvation of the unsaturated metal center and vibrational relaxation. When the experiment is carried out in a longer chain alcohol, however, solvation by both the alkyl site and the hydroxyl site is observed and rearrangement dynamics can be monitored. The difference spectra for $Cr(CO)_6$ in 1-butanol are shown in Figure 9. Four distinct absorptions are seen in the spectra. These features are attributable to the parent bleach at 1983 cm^{-1}, an alkyl solvated pentacarbonyl complex E band at 1957 cm^{-1}, and two hydroxyl solvated pentacarbonyl absorptions at 1892 and 1935 cm^{-1} corresponding to the A_1 and E bands, respectively. The A_1 band of the alkyl solvated complex is masked by the overlapping E band of the hydroxyl solvated complex and is not observed. At early times, all four features are present and at increasing time delays the intensities of the absorptions from the alkyl solvated species decrease and those from the hydroxyl solvated species increase. Kinetic traces for the decay of the alkyl bound complex and the rise of the hydroxyl bound complex are shown in Figure 10. These processes are concomitant with similar time constants of 244.2 ± 20.7 and 314.0 ± 41.9 ps, respectively.[36] The

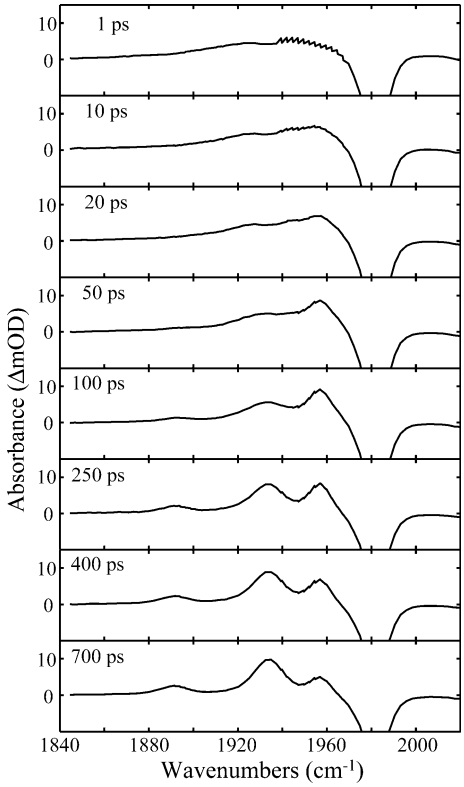

Figure 9. UV-pump, IR-probe spectra of chromium hexacarbonyl in neat 1-butanol at increasing delay times after photoexcitation.

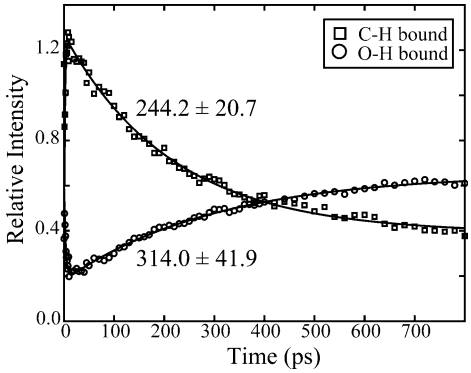

Figure 10. Experimental kinetic data for chromium hexacarbonyl in 1-butanol. The experimental data are obtained by fitting the spectra of $Cr(CO)_5$−butanol with the sum of spectra of $Cr(CO)_5$−methanol (OH-bound) and $Cr(CO)_5$−pentane (CH-bound) according to eq 1. Kinetic traces of the alkyl bound complex (open squares) and the hydroxyl bound complex (open circles) are shown with single-exponential fits to the data (solid lines). Time constants for the exponential fits are shown beside each trace.

similarity of the decay time for the alkyl solvated species and the rise time of the hydroxyl solvated as well as the isosbestic point that is observed at 1946 cm^{-1} indicates that these are related processes. This is consistent with the expectation for this process, namely, that the weakly bound alkyl solvated complex will eventually rearrange to form the more stable hydroxyl bound species.

The only experiments carried out in alcohol solutions that do not exhibit the rearrangement described for 1-butanol are methanol, as mentioned above, and ethanol. The reason for the lack of rearrangement in these solvents is attributed to the inability to see distinct absorptions in the first 30 ps after photoexcitation. At very early times, the metal carbonyl species is vibrationally excited. This excess energy results in absorptions that are broad and red shifted as compared with the species in its vibrational ground state.[37] Further, since the quantum yield of carbonyl loss is not 1.00, there will be a population of excited parent molecules.[38] These excited species will have absorptions that are red shifted with respect to the parent bleach. This is the same region as the alkyl solvated species absorbs and, therefore, it is reasonable to expect that the population of alkyl solvated complexes will be masked by vibrational relaxation. Because there are very few alkyl sites for the metal center to sample, the rearrangement occurs on a time scale that is comparable to vibrational relaxation and is therefore not directly observable. Simulations of these two solvent systems using the model discussed below give rearrangement times that are extremely fast in agreement with the experimental observations.

TABLE 2: Time Constants for Exponential Fits to Experimental Data[a]

alcohol	decay of M−CH complex (ps)	rise of M−OH complex (ps)
1-propanol	223.0 ± 9.9	225.7 ± 11.2
2-propanol	101.8 ± 3.9	101.9 ± 5.6
1-butanol	244.2 ± 20.7	314.0 ± 41.9
2-butanol	198.9 ± 10.7	161.3 ± 10.3
isobutanol	377.7 ± 37.8	427.4 ± 46.8
1-pentanol	69.6 ± 27.1	23.0 ± 17.5
	461.5 ± 415.0	440.1 ± 162.6
2-pentanol	324.5 ± 55.0	243.5 ± 32.8
2-methylbutanol	440.5 ± 95.2	402.5 ± 82.8
3-methylbutanol	480.9 ± 143.6	342.6 ± 58.3

[a] In all alcohol solutions the absorption from the alkyl solvated metal complex decays with a concommitant rise in the absorption from the hydroxyl solvated metal complex.

All of the other alcohol solutions demonstrate difference spectra that are very similar to that shown for 1-butanol. The main difference between the solvents is the rearrangement time. Table 2 lists the decay time of the alkyl solvated absorption centered around 1957 cm^{-1} and the rise time of the hydroxyl solvated absorption centered around 1935 cm^{-1}. In cases where only one time constant is given, a single exponential function was used to fit the data. In cases where two time constants are provided, the data were fit to a double exponential. The disparity between data fit with a single exponential and data fit with a double exponential is related to the properties of the solvent. Since vibrational energy relaxation is a solvent dependent property, it is not always directly appropriate to use the spectra from pentane and methanol solutions to fit the data in a long chain alcohol. Further, the parent bleach and product absorptions are shifted slightly depending on the solvent environment. Thus, fitting the spectra of $Cr(CO)_6$ in a long chain alcohol with the spectra in methanol and pentane results in some inherent error.

In assigning a mechanism to the experimental data, it is useful to group the data according to the expected results from each mechanism. In Figure 11A the experimental data are grouped according to the number of carbon atoms in the alcohol; if such a grouping scheme were appropriate, a stochastic mechanism would be most logical. In Figure 11B the experimental data are grouped according to the number of carbon atoms from one end of the alkyl chain to the hydroxyl group. Branched molecules are plotted multiple times since they can have more than one distance associated with them. If a chainwalk mechanism is the best description of the reaction, then it would be expected that alcohols having the same number of carbon atoms from one end of the alkyl chain to the hydroxyl group would have similar rearrangement times. Inspection of these plots indicates that while the general trend of increasing rearrangement time for increasing chain length are observed in both plots, a

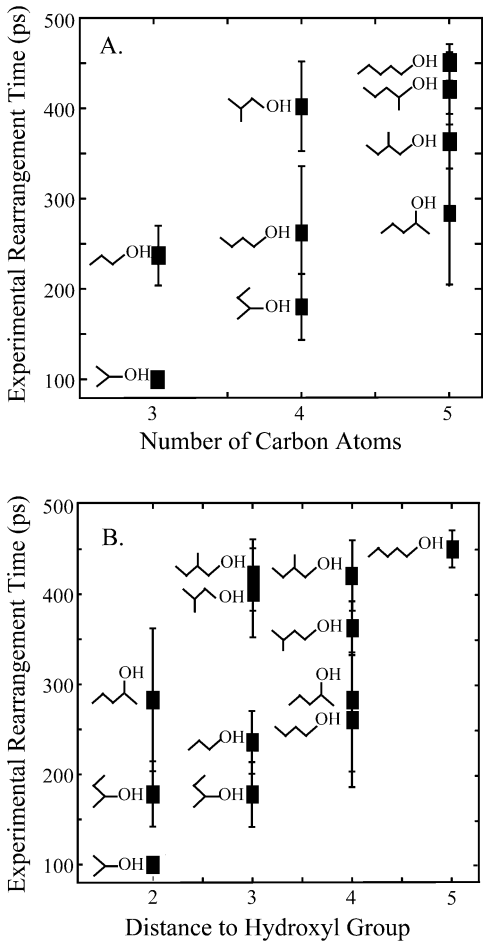

Figure 11. Experimental rearrangement times grouped according to the number of carbon atoms in the alcohol (A) and according to the distance from the end of the alkyl chain to the hydroxyl site (B).

simple assignment to one of these two possible mechanisms cannot be made based on these groupings alone.

A more quantitative analysis of this type can be made using a population matrix that is propagated in time using a connection matrix consistent with the alcohol and the simulation type. For example, in all alcohols and all simulation types the initial population will be equally distributed among the alkyl sites and the alcohol site because we suppose that the initial solvation site is random. Population from the hydroxyl site increases with time but cannot be removed. In the stochastic simulation, population from each of the alkyl sites will be transferred to each of the other sites. Eventually, all of the population will be confined to the hydroxyl site and the simulation will end; the simulations shown here are complete when 99% of the population is in the hydroxyl well. The first step of the stochastic matrix propagation process for 1-butanol is

$$\begin{bmatrix} \mathrm{OH} & \mathrm{C}_\alpha & \mathrm{C}_\beta & \mathrm{C}_\gamma & \mathrm{C}_\delta \\ \frac{1}{5} & \frac{1}{5} & \frac{1}{5} & \frac{1}{2} & \frac{1}{5} \end{bmatrix} \cdot \begin{bmatrix} & \mathrm{OH} & \mathrm{C}_\alpha & \mathrm{C}_\beta & \mathrm{C}_\gamma & \mathrm{C}_\delta \\ \mathrm{OH} & 1 & 0 & 0 & 0 & 0 \\ \mathrm{C}_\alpha & \frac{1}{5} & \frac{1}{5} & \frac{1}{5} & \frac{1}{5} & \frac{1}{5} \\ \mathrm{C}_\beta & \frac{1}{5} & \frac{1}{5} & \frac{1}{5} & \frac{1}{5} & \frac{1}{5} \\ \mathrm{C}_\gamma & \frac{1}{5} & \frac{1}{5} & \frac{1}{5} & \frac{1}{5} & \frac{1}{5} \\ \mathrm{C}_\delta & \frac{1}{5} & \frac{1}{5} & \frac{1}{5} & \frac{1}{5} & \frac{1}{5} \end{bmatrix}$$

In the chainwalk simulation, the process is the same, but the propagation matrix is different. The population will move to an adjacent site with each propagation step. The first step for the chainwalk matrix propagation process for 1-butanol is

$$\begin{bmatrix} \mathrm{OH} & \mathrm{C}_\alpha & \mathrm{C}_\beta & \mathrm{C}_\gamma & \mathrm{C}_\delta \\ \frac{1}{5} & \frac{1}{5} & \frac{1}{5} & \frac{1}{5} & \frac{1}{5} \end{bmatrix} \cdot \begin{bmatrix} & \mathrm{OH} & \mathrm{C}_\alpha & \mathrm{C}_\beta & \mathrm{C}_\gamma & \mathrm{C}_\delta \\ \mathrm{OH} & 1 & 0 & 0 & 0 & 0 \\ \mathrm{C}_\alpha & \frac{1}{2} & 0 & \frac{1}{2} & 0 & 0 \\ \mathrm{C}_\beta & 0 & \frac{1}{2} & 0 & \frac{1}{2} & 0 \\ \mathrm{C}_\gamma & 0 & 0 & \frac{1}{2} & 0 & \frac{1}{2} \\ \mathrm{C}_\delta & 0 & 0 & 0 & 1 & 0 \end{bmatrix}$$

The number of propagation steps required for the complete movement of population into the hydroxyl site is shown for each alcohol studied in Table 3.

TABLE 3: Number of Steps for 99% of the Starting Population To Reach the Hydroxyl Site via the Matrix Propagation Method Described in the Text[a]

alcohol	stochastic (steps)	chainwalk (steps)
1-propanol	25	34
2-propanol	25	29
1-butanol	31	55
2-butanol	31	44
isobutanol	31	45
1-pentanol	38	81
2-pentanol	38	67
2-methylbutanol	38	67
3-methylbutanol	38	66

[a] Stochastic simulations carry no information about the structure (linear, branched) of the molecule and so give identical results for molecules of the same length.

The results using the propagation matrix provide a simple way to group the data in order to assign a particular rearrangement mechanism to the data. Correlation graphs of the matrix simulation results plotted against the experimental data are shown in Figure 12 for each of the solvent systems studied. Figure 12A shows the experimental data plotted against the stochastic matrix propagation results. Figure 12B shows the experimental data graphed against the chainwalk matrix propagation results. Although the chainwalk matrix propagation results reflect the experimental data more closely than the stochastic results, neither of the models provides good agreement with the experiments.

Since neither of these two grouping schemes definitively identifies the mechanism for the ligand rearrangement, the experimental results alone cannot be used to assign a particular mechanistic description to this process. One reason for this is that such a simple inspection does not take into account the effects of the bath on the rearrangement process. In particular, solvent viscosity is expected to be strongly linked to the time scale for dissociation of an alkyl bound solvent molecule. This is because the viscosity is the solvent parameter that characterizes the friction coefficient and allows for diffusive motion along the barrier as described by the Langevin equation. Simulations, therefore, were carried out for all of the solvent systems studied experimentally to account for the influence of the environment. Kinetic data were obtained by fitting the population of hydroxyl bound complexes over time with a single-exponential function. Examples of a group of simulated data sets and the resulting single-exponential fits are shown in Figure 13 for 1-butanol. The results of simulations for all of the solvent systems studied are given in Table 4. In Figure 14 all of the simulation data

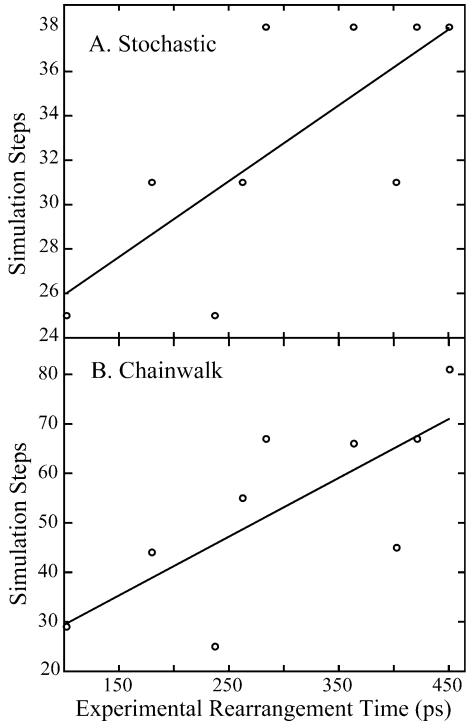

Figure 12. Experimental rearrangement times plotted against the number of matrix propagation steps required for the entire population to be solvated at the hydroxyl site. Matrix propagation results for the stochastic simulation (A) and the chainwalk simulation (B) are shown. The solid line is a linear fit to the data demonstrating a nonlinear relationship and each point represents the rearrangement of chromium pentacarbonyl in one of the nine solvents as described in the text.

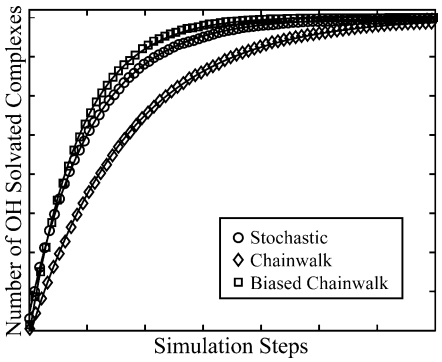

Figure 13. Simulation kinetic traces for $Cr(CO)_5$ in 1-butanol. Circles represent stochastic simulation results, diamonds represent chainwalk results, and squares represent biased chainwalk results. Single-exponential fits are overlayed onto the data. The *y*-axis represents the percentage of $Cr(CO)_5$ complexes that are bound to the hydroxyl group of the alcohol. Numbers and units are not given in order to deemphasize quantitative results and emphasize qualitative trends.

from Table 4 are plotted against the experimental data. Linear fits to each of the plots give goodness of fit values that range from 0.651 to 0.756. While the biased chainwalk mechanism gives the best correlation between the experimental and simulation data, none of the goodness of fit values is sufficiently close to 1.0 to allow for confident assignment of one mechanism over the other.

Although the slope of the correlation graph in Figure 14 also implies that the biased chainwalk mechanism best fits the experimental results, it is important to remember that numerical values from the simulations should not be used quantitatively because of simplifications in the model. For example, the use of a cosine potential will systematically change the number of steps required in the simulation which means that the trends in

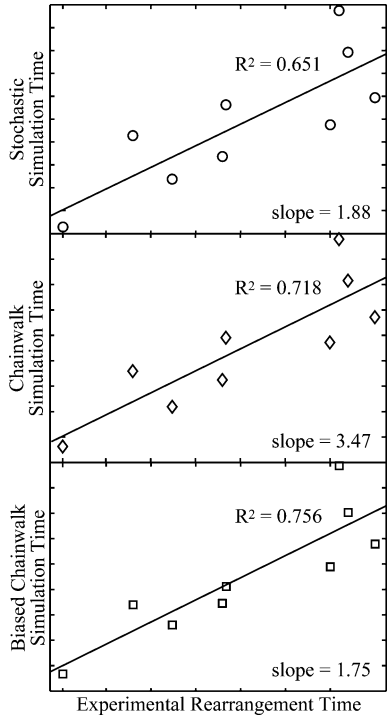

Figure 14. Experimental data plotted versus simulation data for each solvent studied. The line from a linear-least-squares analysis is shown along with the slope and the goodness of fit value for each simulation type. The *y*-axis represents the number of simulation steps required for all complexes to be bound to the hydroxyl group. The *x*-axis is the experimental rearrangement time obtained by averaging the fits for the decay of alkyl bound complexes and the rise of hydroxyl bound complexes. Numbers and units are not given in order to deemphasize quantitative results and emphasize qualitative trends.

TABLE 4: Average Simulation Time for Hydroxyl Coordination.

alcohol	stochastic (ps)	chainwalk (ps)	biased chainwalk (ps)
1-propanol	437.2 ± 16.9	636.2 ± 52.8	360.4 ± 22.4
2-propanol	228.4 ± 17.8	325.6 ± 21.0	167.1 ± 14.2
1-butanol	535.8 ± 38.1	847.8 ± 44.8	445.4 ± 31.8
2-butanol	627.3 ± 37.5	918.7 ± 67.9	439.4 ± 29.7
isobutanol	675.9 ± 33.4	1143.9 ± 38.5	589.1 ± 22.2
1-pentanol	792.9 ± 35.0	1343.0 ± 57.7	678.4 ± 31.9
2-pentanol	762.2 ± 60.7	1181.5 ± 69.1	511.1 ± 43.6
2-methylbutanol	992.0 ± 38.2	1629.7 ± 103.5	802.9 ± 39.0
3-methylbutanol	1174.0 ± 78.3	1956.3 ± 128.9	986.8 ± 69.0

[a] All averages are the result of 10 simulation sets of 500 particles each. Errors are the standard deviation from the ten independent simulation sets.

the data are more informative. Figure 15 shows the results of each simulation type for the nine solvents studied. The trend in the experimental values is well simulated by all three mechanisms, and within the errors of the experiment, none of the simulation types can be definitively assigned to the experimental observations.

To understand why the results from all three simulation types are so similar, it is instructive to look at the evolution of a delta function distribution for the initial solvation site and position in the well. In these sets of simulations, the particles are initially placed in the center of the γ carbon well and then allowed to evolve according to the procedures described above. Figure 16 shows the evolution of the distributions for each of the three simulation types. The first time slice shows the delta distribution after 20 simulation steps. Each subsequent time slice shows the distribution after an additional 20 simulation steps. In all three

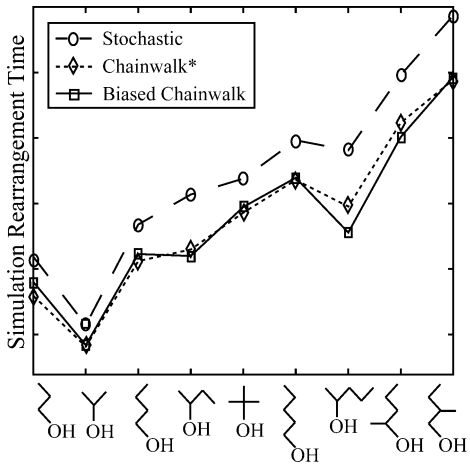

Figure 15. Simulation data for all alcohol solvents. The number of simulation steps is plotted against the solvent species. Numbers and units are not given in order to deemphasize quantitative results and emphasize the trends in the simulation results. *Note that the chainwalk simulation times have been divided by 2 to allow for comparison of the trend.

of the simulation types, it is observed that the distribution quickly randomizes itself. In fact, the distributions for the three simulation sets are very similar in the last time slice shown (160 simulation steps) with the main difference being the time required for all particles to become trapped in the hydroxyl well. Further, because the reaction is highly diffusive, the stochastic simulation does not differ much from either of the chainwalk simulations. Since the population distribution is quickly randomized and the alkyl well depths are very similar for all of the alcohols studied, the simulation results do not show a clear distinction between the rearrangement types. These results suggest that the two mechanistic descriptions of linkage isomerization reactions are not adequately distinguishable using Brownian dynamics and an assignment of one or the other based on these simulations alone is not justified.

There are two obvious reasons for the failure of Brownian motion simulations in predicting a single mechanistic description of the ligand rearrangement process. First, it is possible that the actual, physical mechanism is a hybrid of these two extremes. Simply put, the mechanisms are not different when the bath is included in the dynamic behavior. Fluctuations from the bath that result from the viscosity of the solvent as well as the interaction energy between the metal center and the solvent ligand are the determining factors in the rearrangement time. This would mean that the microscopic nature of sampling sites is the fast step and therefore not a determining factor in the time scale in the rearrangement. Second, it may be that the Langevin equation does not adequately simulate the physical behavior of the system. A more sophisticated analysis that incorporates the local solvent structure and its effect on the rearrangement may improve the model. For example, if the first solvent shell is highly ordered, an intermolecular rearrangement process will not actually access all sites along the alcohol chain with equal probability.

To understand if the chainwalk and stochastic descriptions of ligand rearrangement are physically distinguishable and, if so, which label to assign to the process, further work must be carried out. Currently, we are undertaking a series of experiments that investigate the rearrangement of $Cr(CO)_6$ in cyclic alcohol solvents. These solvents are expected to give a more definitive difference between the two mechanisms because while the solvent viscosity does not change significantly, a chainwalk mechanism allows for the possibility of very long rearrangement times. In addition, a more complex model of the rearrangement may be required to test the two possibilities. Molecular dynamics simulations will be required to gain a more thorough understanding of the local solvent environment, and these will be incorporated into the simulation engine to give a more physical description for the sampling of sites in the stochastic simulation.

5. Conclusions

An ensemble measurement of the rearrangement from alkyl bound complexes to hydroxyl bound complexes cannot access the microscopic nature of the ligand rearrangement and cannot, therefore, be used to directly assign a specific mechanism to the process. We expect that the limited ability of these experiments to differentiate between the different mechanisms is due to the effect of the solvent on the nature of the rearrangement process. Computer modeling has been utilized for the first time to explicitly include the bath effects in the dynamical linkage isomerization reactions of metal carbonyl complexes in neat alcohol solutions. The models demonstrate dynamic behaviors that are very similar to each other and preclude a definitive assignment of one mechanism over the other indicating that the reaction is highly diffusive. The time required for solvation by the hydroxyl group is longest in the case of a chainwalk description, but the trend in solvation time as the solvent is varied is not very different for the three simulation types. The conclusion of this work is that the mechanistic labels of intramolecular and intermolecular rearrangement used to describe this process are too similar to be uniquely isolated using the diffusive motion along a barrier alone. Current experimental work is aimed at cyclic alcohol solvents which provide deviations between the two mechanisms. Current theoretical work is aimed at gaining a more physical description of the local solvent environment and incorporating this into the Brownian dynamics model.

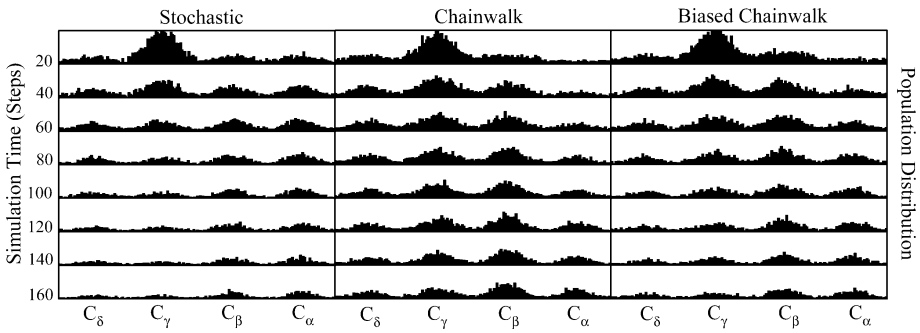

Figure 16. Evolution of population distribution at increasing times after starting at the center of the C_γ well of 1-butanol. Each distribution shown is 20 simulation steps after initialization. Loss of population from the alkyl wells (shown) is transferred into the hydroxyl well (not shown).

Acknowledgment. We thank the National Science Foundation for funding and the Office of Basic Energy Sciences, Chemical Sciences Division, of the U.S. Department of Energy under Contract DE-AC02-05CH11231 for the use of some specialized equipment. The authors also thank Steve Shipman for many helpful discussions and critical reading of the manuscript.

References and Notes

(1) Cotton, F. A.; Wilkinson, G.; Gauss, P. L. In *Basic Inorganic Chemistry*; John Wiley and Sons: Toronto, 1995.
(2) Schultz, R. H. *Int. J. Chem. Kinet.* **2004**, *36*, 427.
(3) Shagal, A.; Schultz, R. H. *Organometallics* **2002**, *21*, 5657.
(4) Ladogana, S,; Nayak, S. K.; Smit, J. P.; Dobson, G. R. *Inorg. Chem.* **1997**, *36*, 650.
(5) Xie, X.; Simon, J. D. *J. Am. Chem. Soc.* **1990**, *112*, 1130.
(6) Hall, C.; Perutz, R. N. *Chem. Rev.* **1996**, *96*, 3125.
(7) Lawes, D. J.; Geftakis, S.; Ball, G. E. *J. Am. Chem. Soc.* **2005**, *127*, 4134.
(8) Snee, P. T.; Payne, C. K.; Mebane, S. D.; Kotz, K. T.; Harris, C. B. *J. Am. Chem. Soc.* **2001**, *123*, 6909.
(9) Simon, J. D.; Xie, X. *J. Phys. Chem.* **1989**, *93*, 291.
(10) Kotz, K. T.; Yang, H.; Snee, P. T.; Payne, C. K.; Harris, C. B. *J. Organomet. Chem.* **2000**, *596*, 183.
(11) Zhang, S.; Zang, V.; Bajaj, H. C.; Dobson, G. R.; van Eldik, R. *J. Organomet. Chem.* **1990**, *397*, 279.
(12) Schulten, K.; Schulten, Z.; Szabo, A. *J. Chem. Phys.* **1981**, *74*, 4426.
(13) Wagner, C.; Kiefhaber, T. *Proc. Natl. Acad. Sci. U.S.A.* **1999**, *96*, 6716.
(14) Shanoski, J. E.; Payne, C. K.; Kling, M. F.; Glascoe, E. A.; Harris, C. B. *Organometallics* **2005**, *24*, 1852.
(15) Frisch, M. J.; Trucks, G. W.; Schlegel, H. B.; Scuseria, G. E.; Robb, M. A.; Cheeseman, J. R.; Zakrzewski, V. G.; Montgomery, J. A., Jr.; Stratmann, R. E.; Burant, J. C.; Dapprich, S.; Millam, J. M.; Daniels, A. D.; Kudin, K. N.; Strain, M. C.; Farkas, O.; Tomasi, J.; Barone, V.; Cossi, M.; Cammi, R.; Mennucci, B.; Pomelli, C.; Adamo, C.; Clifford, S.; Ochterski, J.; Petersson, G. A.; Ayala, P. Y.; Cui, Q.; Morokuma, K.; Rega, N.; Salvador, P.; Dannenberg, J. J.; Malick, D. K.; Rabuck, A. D.; Raghavachari, K.; Foresman, J. B.; Cioslowski, J.; Ortiz, J. V.; Baboul, A. G.; Stefanov, B. B.; Liu, G.; Liashenko, A.; Piskorz, P.; Komaromi, I.; Gomperts, R.; Martin, R. L.; Fox, D. J.; Keith, T.; Al-Laham, M. A.; Peng, C. Y.; Nanayakkara, A.; Challacombe, M.; Gill, P. M. W.; Johnson, B.; Chen, W.; Wong, M. W.; Andres, J. L.; Gonzalez, C.; Head-Gordon, M.; Replogle, E. S.; Pople, J. A. *Gaussian 98*, revision A.11.4; Gaussian, Inc.: Pittsburgh, PA, 2002.
(16) Becke, A. D. *J. Chem. Phys.* **1993**, *98*, 5648.
(17) Lee, C. T.; Yang, W. T.; Parr, R. G. *Phys. Rev. B* **1988**, *37*, 785.
(18) Stephes, P. J.; Devlin, F. J.; Chabalowski, C. F.; Frisch, M. J. *J. Phys. Chem.* **1994**, *98*, 11623.
(19) Hehre, W. J.; Ditchfie, R.; Pople, J. A. *J. Chem. Phys.* **1972**, *56*, 2257.
(20) Francl, M. M.; Pietro, W. J.; Hehre, W. J.; Binkley, J. S.; Gordon, M. S.; Defrees, D. J.; Pople, J. A. *J. Chem. Phys.* **1982**, *77*, 3654.
(21) Hay, P. J.; Wadt, W. R. *J. Chem. Phys.* **1985**, *82*, 299.
(22) Farrell, G. J.; Burkey, T. J. *J. Photochem. Photobiol., A* **2000**, *137*, 135.
(23) The results of the simulations show the same trend when a two body reduced mass (based on the metal fragment and the alcohol) is used in the simulation.
(24) Hansen, J. P.; McDonald, I. R. In *Theory of Simple Liquids*; Academic Press: Orlando, FL, 1986.
(25) Ben-Amotz, D.; Scott, T. W. *J. Chem. Phys.* **1987**, *87*, 3739.
(26) Roy, M.; Doraiswamy, S. *J. Chem. Phys.* **1993**, *98*, 3213.
(27) Bauer, D. R.; Brauman, J. I.; Pecora, R. *J. Am. Chem. Soc.* **1974**, *96*, 6840.
(28) Alder, B. J.; Gass, D. M.; Wainwright, T. E. *J. Chem. Phys.* **1970**, *53*, 3813.
(29) Inclusion of local heating effects that result from photoexcitation was attempted by altering the bath temperature at early simulation times. Inclusion of pressure variations (also a result of photoexcitation) in the simulation will change the friction coefficient and should, therefore, have an effect that is similar to increasing the temperature. The simulation results at higher temperature are faster, as expected, but do not show any difference in the trends observed for the various simulation types. Consequently, all simulations reported here were carried out in room temperature solutions.
(30) Viswanath, D. S.; Natarajan, G. In *Data Book on the Viscosity of Liquids*; Hemisphere Publishing Corp.: New York, 1989.
(31) Allen, M. P.; Tildesley, D. J. In *Computer Simulation of Liquids*; Oxford University Press: Oxford, 1987.
(32) To verify these statements, simulations were carried out with ±5−10% of the binding energy added to the DFT results. The rearrangement times for these simulations showed trends that are consistent with those reported in this work.
(33) Lian, T.; Bromberg, S. E.; Asplund, M. C.; Yang, H.; Harris, C. B. *J. Phys. Chem.* **1996**, *100*, 11994.
(34) Joly, A. G.; Nelson, K. A. *Chem. Phys.* **1991**, *152*, 69.
(35) Dougherty, T. P.; Heilweil, E. J. *Chem. Phys. Lett.* **1994**, *227*, 19.
(36) The discrepancies between the time constants for the decay of the alkyl absorption and the rise of the hydroxyl absorption are a result of the fitting routine used in the data analysis. Since the solvent environment influences the absorption frequencies of the parent species and intermediate complexes, there is an inherent error in the fits which is not accounted for in the reported fit errors which only reflect the confidence interval of the fit to the data.
(37) King, J. C.; Zhang, J. Z.; Schwartz, B. J.; Harris, C. B. *J. Chem. Phys.* **1993**, *99*, 7595.
(38) Nayak, S. K.; Burkey, T. J. *Organometallics* **1991**, *10*, 3745.